Article

Design, Synthesis, and Docking Study of Acyl Thiourea Derivatives as Possible Histone Deacetylase Inhibitors with a Novel Zinc Binding Group

Duraid H. Al-Amily *[ID] **and Mohammed Hassan Mohammed**

Department of Pharmaceutical Chemistry, College of Pharmacy, University of Baghdad, Baghdad 10047, Iraq; dr.mhassanm666666@yahoo.com
* Correspondence: colrelated@copharm.uobaghdad.edu.iq

check for updates

Abstract: Histone deacetylase inhibitors with zinc binding groups often exhibit drawbacks like non-selectivity or toxic effects. Thus, there are continuous efforts to modify the currently available inhibitors or to discover new derivatives to overcome these problems. One approach is to synthesize new compounds with novel zinc binding groups. The present study describes the utilization of acyl thiourea functionality, known to possess the ability to complex with metals, to be a novel zinc binding group incorporated into the designed histone deacetylase inhibitors. *N*-adipoyl monoanilide thiourea (**4**) and *N*-pimeloyl monoanilide thiourea (**5**) have been synthesized and characterized successfully. They showed inhibition of growth of human colon adenocarcinoma and mouse hepatoblastoma cells with low cytotoxic effect against normal human breast cells. Their binding mode to the active site of several histone deacetylases has been studied by docking and the results gave a preliminary indication that they could be successful histone deacetylase inhibitors.

Keywords: histone deacetylase inhibitors; acyl thiourea derivatives; zinc binding group; distance from zinc ion

1. Introduction

Histone deacetylases (HDACs) comprise a class of enzymes that catalyze the deacetylation of the ε-amino groups of lysine residues at the N-termini of histones [1], proteins that act as a core for DNA compaction into nucleosomes that comprise chromatins [2]. The deacetylation process results in the compaction of nucleosomes and subsequently the repression of gene transcription. Many reports demonstrate that HDACs are overexpressed in several types of cancer [3,4]. Therefore, they represent a valuable target for cancer treatment [5].

In mammalian cells, the identified HDACs represent 18 isoforms and they fall into four major classes (I–IV). Class I includes HDAC1, 2, 3, and 8 while class II includes isoforms 4–7, 9 and 10. Isoform 11 represents class IV. These three classes are zinc-dependent in their activity. The remaining seven isoforms depend on the cofactor nicotine adenine dinucleotide rather than zinc for their catalytic activity and comprise class III [6].

The zinc-dependent classes are most commonly investigated and subjected to inhibition studies as an approach for cancer treatment [7]. HDAC2 is a common example, since its crystallographic structure is well resolved [8]. Early studies on the binding site revealed that it is shaped as an internal tunnel-like cavity having a length of 11 Å. At the bottom of this cavity, a zinc ion is positioned followed by a 14 Å foot-like pocket [9] (Figure 1). Lysine residues of histone fit into the tunnel so that they could be deacetylated [10,11].
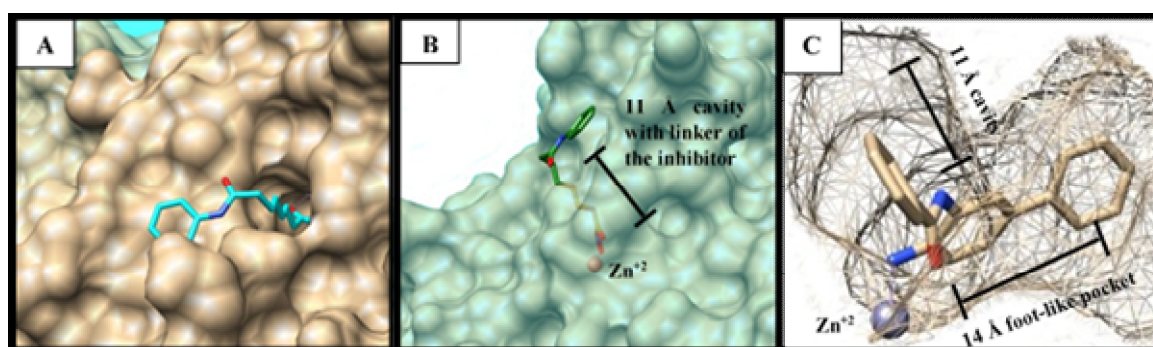
Figure 1. The binding site of histone deacetylase 2. (**A**) The opening of the tunnel cavity is shown in which the linker of the inhibitor (cyan) is lying. (**B**) A side view of the binding site with 30% transparency of the surface to make the whole length of the tunnel (11 Å) visible together with the linker of the inhibitor (forest green). Zinc ion is visible at the deepest end of the tunnel. (**C**) Mesh surface of the binding site showing the inhibitor inside the 14 Å foot-like pocket.

Accordingly, the design of inhibitors for zinc-dependent HDACs should have a zinc binding group (ZBG) to bind to the zinc ion, a linker chain that mimics acetylated lysine of histone to fit into the cavity, and a hydrophobic cap to recognize and interact with the outer surface. These are best illustrated by the classical, FDA-approved inhibitor suberoylanilide hydroxamic acid **1** (SAHA, vorinostat) [12,13].

Other common synthetic inhibitors with ZBG other than hydroxamic acid derivatives include entinostat **2** (MS-275), a benzamide, and the short-chain aliphatic carboxylic acid, valproic acid **3** (Figure 2).
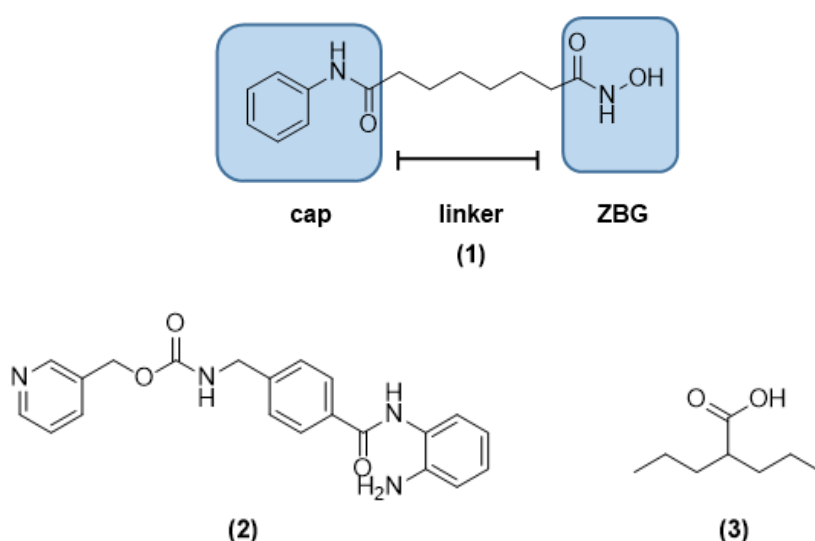

Figure 2. Common histone deacetylase inhibitors with zinc binding group.

The most common disadvantages encountered with these classes of inhibitors are related to the poor pharmacokinetic profile and enzyme non-specificity of hydroxamates, in vivo toxicity of benzamides due to the free *o*-amine group, and the weak binding of the carboxylic acids to zinc ion [5]. These problems encouraged us to design new compounds that keep both the hydrophobic cap and linker but with a new, unique ZBG.

Acyl thiourea derivatives can coordinate metals in either a bidentate fashion through both the carbonyl oxygen and the thiocarbonyl sulfur [14,15], or a monodentate fashion via the thiocarbonyl sulfur only [16,17] (Figure 3). Thiourea itself can coordinate metals through its sulfur or through one of its nitrogen atoms [18–20].
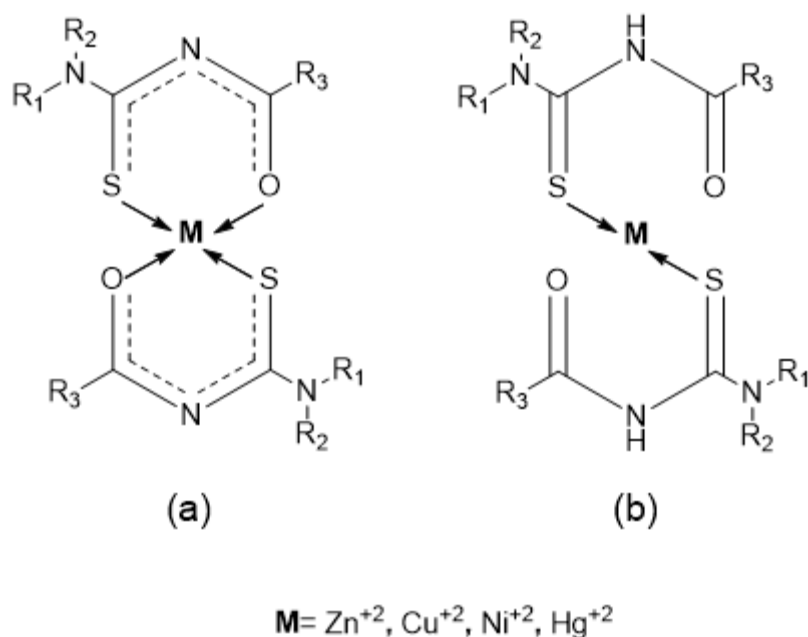
M= Zn⁺², Cu⁺², Ni⁺², Hg⁺²

Figure 3. Coordination modes of acyl thiourea derivative with metal ions as bidentate (**a**) or monodentate (**b**).

Here, we wish to describe for the first time the synthesis of two novel substituted acyl thiourea derivatives (compounds **4** and **5**, Figure 4) as possible inhibitors for zinc-dependent histone deacetylase enzymes. They have the acyl thiourea functionality as a unique ZBG, a 4- or 5-carbon linker, and an aromatic capping group.
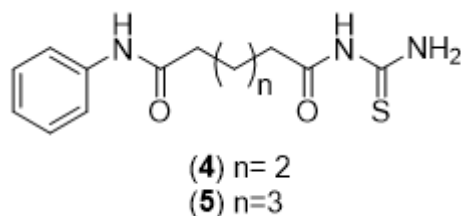

(4) n= 2
(5) n=3

Figure 4. The designed compounds with acyl thiourea functionality as a zinc binding group.

In order to demonstrate whether these compounds could have cytotoxicity activity, an in vitro cytotoxicity assay was carried out against HRT-18 cell line (human colon adenocarcinoma) and HC-04 cell line (mouse hepatoblastoma). Besides, they have been subjected to a docking study against several histone deacetylase enzymes and their binding parameters have been compared to those obtained from docking of **1** against the same enzymes.

2. Materials and Methods

Reagents and solvents were used for chemical synthesis as obtained from the supplier (Sigma-Aldrich (St. Louis, MO, USA), Fluka (Charlotte, NC, USA), Romil (Cambridge, UK), GCC Diagnostics (Deeside, UK), ReagentWorld (Ontario, CA, USA), and Thomas-Baker (Mumbai, India). Melting points were measured using the Stuart SMP3 melting point apparatus (UK) and are uncorrected. Thin-layer chromatography was achieved using 0.2 mm pre-coated TLC-sheets Alugram® Xtra SIL G/UV254 (Macherey-Nagel, Germany) and the visualization was under a 254 nm UV lamp. FT-IR spectroscopy was done using Shimadzu IRAffinity-1 Spectrometer (Shimadzu, Japan) and Specac® Quest ATR- diamond type (Specac Ltd., Kent, UK) at the University of Baghdad-College of Pharmacy. ¹H-NMR and ¹³C-NMR analysis was performed at 400 MHz and 100 MHz respectively (d_6-DMSO as

the solvent) using The Bruker Avance III, 400 MHz spectrometer (Billerica, MA, USA) at Sophisticated Test and Instrumentation Centre (Cochin University of Science and Technology, Cochin, India), with the chemical shifts (δ) expressed in parts per million (Supplementary File 1). Elemental analysis was carried out using EuroEA 3000 analyzer (EuroVector, Milan, Italy).

Molecular docking was performed using AutoDock Vina software [21] that is integrated into USCF Chimera software [22]. Enzymes crystallized structures were retrieved from the protein data bank (PDB, www.rcsb.org) [23].

Cytotoxicity assay was performed at the iRAQ Biotech laboratories using trypsin/EDTA, RPMI 1640, fetal bovine serum (Capricorn, Germany); 3-(4,5-dimethyl-2-thiazolyl)-2,5-diphenyl -2H-tetrazolium bromide (MTT stain-Bio-World, Dublin, OH, USA); dimethyl sulfoxide (DMSO-Santacruz Biotechnology, Dallas, TX, USA); CO_2 incubator and laminar flow hood (Cypress Diagnostics, Hulshout, Belgium); microtiter reader (Gennex lab., Srinagar Colony Hyderabad, India); cell culture plates (Santa Cruz Biotechnology).

2.1. Chemical Synthesis (Scheme 1)

2.1.1. General Synthesis of Adipic and Pimelic Anhydrides (**4b** and **5b**)

Adipic acid (**4a**) or pimelic acid (**5a**) (27.4 mmol of each) was suspended in acetic anhydride (3 mL/g) and refluxed for 1 h. The solvent was then evaporated under reduced pressure to obtain a semisolid mixture of **4b** and **4c**, or **5b** and **5c**, which was used as such in the next step. FT-IR (ATR; υ, cm^{-1}): 1801, 1739 for **4b** and 1813, 1743 for **5b** (sym. and asym. C=O respectively).

2.1.2. General Synthesis of Monosodium Adipic Monoanilide and Monosodium Pimelic Monoanilide (**4d** and **5d**)

The obtained mixture of **4b** and **4c**, or **5b** and **5c** was dissolved in 10 mL of dry DMF in a round bottom flask that was equipped with a calcium chloride tube and cooled to 0 °C. Then, 3 mL of aniline (32.88 mmol) were added gradually with continuous stirring and cooling. The mixture was then kept stirred at room temperature for 24 h. The mixture was then acidified with 5 N hydrochloric acid, diluted to about 300 mL with cold water, and filtered. The precipitate was washed with water (3 × 50 mL). Then, it was suspended in no more than 50 mL of ice-cooled water and the pH of this mixture was raised to 7 by a dropwise addition of 0.5 N sodium hydroxide solution at 0 °C. The mixture was stirred for 30 min at 0 °C while maintaining this pH by addition of 0.5 N sodium hydroxide solution as needed. Then, the mixture was filtered and the filtrate was evaporated to dryness.

Compound **4d**: off-white powder, yield 35% relative to **4a**, m. p. 259.5–263.8 °C. FT-IR (ATR; υ, cm^{-1}): 3332 (aromatic NH), 3062 (aromatic C–H), 2939 (asym. CH_2), 2866 (sym. CH_2), 1666 (amide C=O), 1600 (aromatic C–C), 1562 (asym. carboxylate C=O), 1539 and 1500 (aromatic C–C), 1431 (sym. carboxylate C=O).

Compound **5d**: off-white powder, yield 25.5% relative to **5a**, m. p. 214-217 °C. FT-IR (ATR; υ, cm^{-1}): 3290 (aromatic NH), 3078 (aromatic C–H), 2920 (asym. CH_2), 2858 (sym. CH_2), 1654 (amide C=O), 1597 (aromatic C–C), 1558 (asym. carboxylate C=O), 1543 and 1496 (aromatic C–C), 1435 (sym. carboxylate C=O).

2.1.3. General Synthesis of Adipic Monoanilide Acid Chloride and Pimelic Monoanilide Acid Chloride (4e and 5e)

Compound **4d** or **5d** (4 mmol) was suspended in 15 mL dry dichloromethane in a round bottom flask that was equipped with a calcium chloride tube and cooled in an ice bath. Pyridine (4 mmol, 0.32 mL) was added followed by a dropwise addition of 0.34 mL of thionyl chloride (4.8 mmol) with continuous stirring and cooling for 10 min. The mixture was then allowed to warm to room temperature with continuous stirring for 30 min. Then, the precipitate formed was collected using

Büchner funnel. The precipitate was washed with dry dichloromethane (3 × 10 mL) during filtration. The white solid mass obtained (in both cases of **4e** and **5e**) was used as such in the next step.

2.1.4. General Synthesis of Adipic Monoanilide Isothiocyanate and Pimelic Monoanilide Isothiocyanate (4f and 5f)

A solution of ammonium thiocyanate (4 mmol, 0.3 g), dissolved in 5 mL dry acetone, was added gradually with stirring to 10 mL of a suspension of the precipitate obtained from the previous step (**4e** or **5e**) in dry acetone. The reaction flask, equipped with a calcium chloride tube, was refluxed for two hours. Then, the solvent was evaporated under reduced pressure and the residue was suspended in 10 mL dry dichloromethane and filtered. After evaporation of the filtrate under reduced pressure, a yellow oil was obtained for both **4f** and **5f** and was used directly in the next step.

2.1.5. General Synthesis of N-Adipoyl Monoanilide Thiourea and N-Pimeloyl Monoanilide Thiourea (4 and 5)

The oily residue from the previous step (**4f** or **5f**) was dissolved in 150 mL dry chloroform and transferred into a Drechsel gas bottle containing a stirring bar and connected to a gas delivery tube, the other end of which was connected to a drying column containing calcium oxide. This column was fit through its ground glass ending onto a flask containing 100 mL of strong ammonia solution. On gently warming the flask (35–40 °C), a continuous stream of dry ammonia gas was bubbled into the chloroform solution of the isothiocyanate (**4f** or **5f**) for 1 h with continuous stirring. Then, the solvent was removed under reduced pressure and the residue was washed with 10 mL ice-cooled water, filtered, and the precipitate was washed again with 10 mL of 5% sodium bicarbonate solution and filtered (twice) yielding a yellow precipitate for both **4** and **5**.

Compound **4**: yellow powder, yield 43% relative to **4d**, m. p. 159.6–166.6 °C. R_f 0.63 (dichloromethane: ethyl acetate; 6:4). FT-IR (ATR; υ, cm^{-1}): 3387 (asymmetric NH$_2$) 3329 (*sec*-amide NH), 3197 (symmetric NH$_2$), 3043 (aromatic C-H), 2920 (asymmetric CH$_2$), 2850 (symmetric CH$_2$), 1705 (acyl thiourea C=O), 1662 (aromatic amide C=O), 1589, 1523 and 1500 (aromatic C-C), 1149 (C=S). ^{1}H-NMR (δ, ppm): 1.56 (m, -CH$_2$-CH$_2$-, 4H), 2.07 (t, aliphatic -CH$_2$-C(O)-, 2H), 2.3 (t, aromatic -CH$_2$-C(O)-, 2H), 7.02 (t, *p*-CH, 1H), 7.28 (t, *m*-CH, 2H), 7.58 (d, *o*-CH, 2H), 9.34 (br, NH$_2$, 1H d_6-DMSO exchangeable), 9.64 (br, NH$_2$, 1H d_6-DMSO exchangeable), 9.86 (s, -NH-, 1H), 11.06 (-CONHCS-, 1H d_6-DMSO exchangeable). ^{13}C-NMR (δ): 24.56, 24.83, 35.53, 36.07, 119.03, 122.95, 128.60, 139.22, 170.96, 174.43, 174.49. Elemental analysis (%) for C$_{13}$H$_{17}$N$_3$O$_2$S: calculated C, 55.89; H, 6.13; N, 15.04; S, 11.48; found C, 55.82; H, 6.21; N, 14.95; S, 11.55.

Compound **5**: yellow powder, yield 48% relative to **5d**, m. p. 144.9–152.4 °C. R_f 0.69 (dichloromethane: ethyl acetate; 6:4) FT-IR (ATR; υ, cm^{-1}): 3352 (asymmetric NH$_2$) 3313 (*sec*-amide NH), 3190 (symmetric NH$_2$), 3043 (aromatic C-H), 2939 (asymmetric CH$_2$), 2850 (symmetric CH$_2$), 1705 (acyl thiourea C=O), 1662 (aromatic amide C=O), 1589, 1523 and 1500 (aromatic C-C), 1149 (C=S). ^{1}H-NMR (δ, ppm): 1.28 (m, -CH$_2$-, 2H), 1.54 (m, -CH$_2$-, 2H), 2.04 (m, -CH$_2$-, 2H), 2.29 (t, aliphatic -CH$_2$-C(O)-, 2H), 2.37 (t, aromatic -CH$_2$-C(O)-, 2H), 7.02 (t, *p*-CH, 1H), 7.28 (t, *m*-CH, 2H), 7.58 (d, *o*-CH, 2H), 9.32 (br, NH$_2$, 1H d_6-DMSO exchangeable), 9.65 (br, NH$_2$, 1H d_6-DMSO exchangeable), 9.85 (s, -NH-, 1H), 11.04 (-CONHCS-, 1H d_6-DMSO exchangeable). ^{13}C-NMR (δ): 24.77, 24.9, 28.32, 34.94, 36.27, 119.02, 122.92, 128.60, 139.26, 171.23, 174.37, 174.69. Elemental analysis (%) for C$_{14}$H$_{19}$N$_3$O$_2$S: calculated C, 57.32; H, 6.53; N, 14.32; S, 10.93; found C, 57.41; H, 6.43; N, 14.26; S, 11.02.
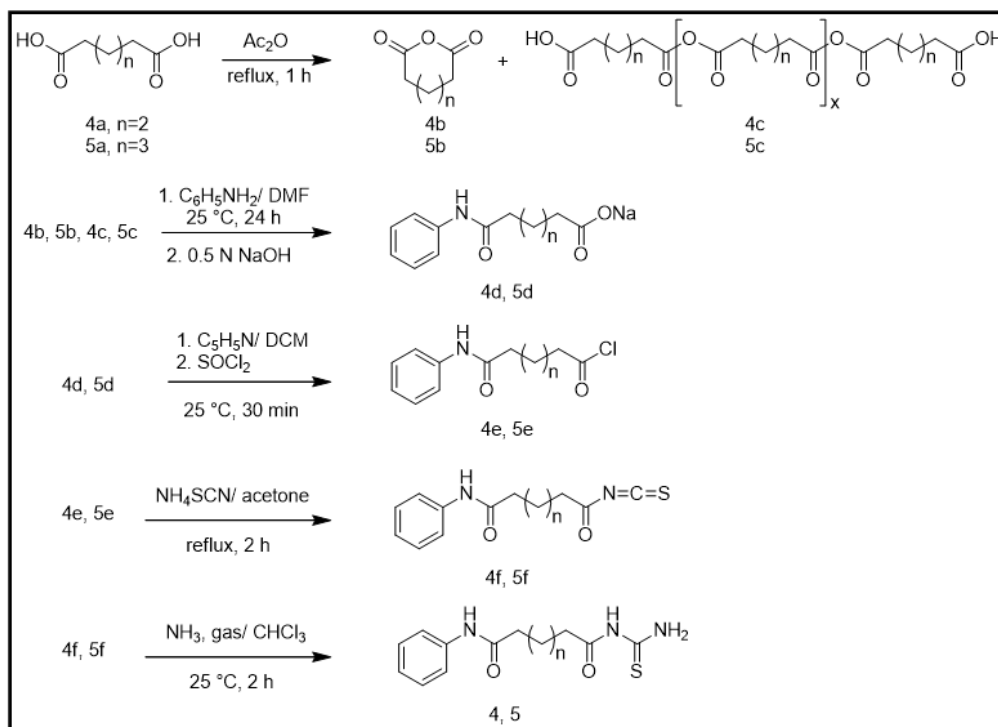
Scheme 1. Synthesis of the target compounds (**4** and **5**).

2.2. *In Vitro Cytotoxicity Study*

2.2.1. Maintenance of Cell Cultures

Human colon adenocarcinoma (HRT-18), mouse hepatic carcinoma (HC-04), and epithelial cells obtained from healthy human breast milk (HBL-100) cell lines were maintained in RPMI-1640 medium that was fortified with solutions of 10% fetal bovine, 100 IU/mL penicillin, and 100 µg/mL streptomycin. The cells were subcultured with Trypsin-EDTA, re-seeded at 80% confluence two times a week, and incubated at 37 °C [24].

2.2.2. Cytotoxicity Assay

MTT cell viability assay was done using 96-well plates. The cell lines were seeded at 1×104 cells/well. After either 24 h or a confluent monolayer was achieved, the cells were treated with compounds **4** and **5** separately at different concentrations (6.25, 12.5, 25, 50, 100 µM). Cell viability was measured after 72 h of treatment by removing the medium, adding 28 µL of 2 mg/mL solution of MTT stain and incubating the cells for 2.5 h at 37 °C. After removing the MTT solution, the crystals remaining in the wells were solubilized by the addition of 130 µL of dimethyl sulfoxide followed by 37 °C incubation for 15 min with shaking [25]. The absorbency was determined on a microplate reader at 492 nm; the assay was performed in triplicate.

The inhibition rate of cell growth (the percentage of cytotoxicity) was calculated according to the following equation:

$$Cytotoxicity(\%) = \frac{A - B}{A} \times 100$$

where A is the optical density of the control and B is the optical density of the sample.

To visualize the shape of cells under an inverted microscope, 200 µL of cell suspensions were seeded in 96-well micro-titration plates at density 1×104 cells/ mL and incubated for 48 h at 37 °C. Then, the medium was removed and each of compounds **4** and **5** was added at its (IC_{50}) separately. After the exposure time, crystal violet solution (50 µL) was used to stain the plates. These plates were then incubated at 37 °C for 15 min followed by gentle washing with water to remove the dye.

A 40× field magnification of an inverted microscope was chosen to examine the cells. Photography was carried out using a digital camera.

2.3. Molecular Docking

The chemical structures of the docked ligands were drawn with ChemBioDraw Ultra 12.0 software and converted into a 3D structure with ChemBio3D Ultra 12.0 software. Then, the ligands were subjected to energy minimization with the latter using its MM2 job, and they were saved as mol2 files. These files were further processed by USCF Chimera software by the addition of Gasteiger charges if applicable.

Only the chain to which the co-crystallized ligand is bound was kept. All unnecessary ions, water molecules, and bound ligands were deleted too. Then, hydrogen atoms were added and Gasteiger charges were assigned to simulate in vivo conditions. The prepared protein was then saved as a mol2 file.

Configuring AutoDock Vina software involved setting the path for the output files (pdbqt and pdb files), assigning center and size values for the search volume (25.709, −15.81, 1.122 for 4LXZ and −6.497, 2.775, −15.65 for 3ZNR), and setting options for both the enzyme and the ligand into their default values. After completion of the docking runs, the scores of enzyme-ligand free energies of binding were obtained with the best pose of each being of the lowest free energy (ΔG). The inhibition constant (K_i) for the best pose of each enzyme-ligand docking was calculated by the equation:

$$K_i = e^{\Delta G}/RT$$

where ΔG is the binding free energy (kcal. Mol^{-1}), R is the gas constant (1.987 cal. mol^{-1}. K^{-1}), and T is the absolute temperature (298.15 K) [26].

3. Results and Discussion

3.1. Chemical Synthesis

Scheme 1 illustrates the synthesis of the target compounds **4** and **5** starting from adipic acid (**4a**) and pimelic acid (**5a**) respectively.

Synthesis of the target compounds (**4** and **5**) was started from adipic acid and pimelic acid respectively (**4a** and **5a**). Heating these dicarboxylic acids in acetic anhydride for 1 h would result in monomeric cyclic anhydrides (**4b** and **5b**). However, these anhydrides are extremely unstable and a portion of the synthesized amount is converted into non-cyclic, polymeric anhydrides (**4c** and **5c**) rapidly during evaporation of the solvent [27,28]. The anhydride mixture (**4b** and **4c**, or **5b** and **5c**) was used as such in the next step which is a modified procedure from previously published works [29,30]. In this step, a slight excess of aniline (1.2 eq. relative to **4a** and **5a**) was added gradually to an ice-cooled solution of the anhydride mixture (in dry DMF) and, then, stirred at room temperature for 24 h. The sodium salts (**4d** and **5d**) were obtained by treatment of the precipitate, resulted after cold acidification of the reaction mixture and filtration, with gradually increasing amounts of ice-cooled NaOH solution (0.5 N) so that the pH was not raised above 7. After filtration and evaporation to dryness, the off-white precipitate (**4d** and **5d**) showed the characteristic FT-IR amide peaks (respectively) at 3332 cm^{-1} and 3290 cm^{-1} (aromatic NH) and at 1666 cm^{-1} and 1654 cm^{-1} (amide carbonyl). Furthermore, the carboxylate peaks were at 1562 cm^{-1} (asym. C=O) and 1431 cm^{-1} (sym. C=O) for **4d** and at 1558 cm^{-1} (asym. C=O) and 1435 cm^{-1} (sym. C=O) for **5d**. These anilides were prepared as sodium salts in order to keep the amide function stable during the next step which involved the synthesis of the acid chlorides **4e** and **5e** using thionyl chloride in the presence of 1 equivalent of pyridine [31], thus avoiding the liberation of HCl. Both of the acid chlorides **4e** and **5e** were used directly in the next step, which involved refluxing them with 1 equivalent of ammonium thoicyanate (relative to **4d** and **5d**) in acetone [32,33] for 2 h to yield the yellow oily isothiocyanates (**4f** and **5f**). These were used directly in the next step, which involved the reaction with gaseous ammonia. This reaction was carried out in a Drechsel gas bottle [34], containing

a chloroform solution of **4f** or **5f** and equipped with a stirring bar, through passing a continuous stream of ammonia gas (dried over a column of soda lime). Chloroform was chosen as the reaction solvent, since ammonia has a considerable solubility in it through hydrogen bond formation [35]. Unlike a previously published work [33], aqueous ammonia solution was not used in order to avoid hydrolysis of **4f** and **5f** into the carboxylic acids of the monoanilides **4d** and **5d** and thiocyanic acid [36].

The FT-IR spectrum of both of the target acyl thioureas (**4** and **5**, obtained as a yellow precipitate) showed a strong peak at 1149 cm^{-1} that might be attributed to thiocarbonyl (C=S) stretching. They also show two peaks that are attributed to the two amide carbonyls; the peak at 1662 cm^{-1} is attributed to the aromatic amide carbonyl stretching for both of them while the peak at 1705 cm^{-1} (for both) is attributed to the aliphatic amide carbonyl stretching [37–39]. The latter's unusually-high amide carbonyl stretching frequency is probably due to the lone pair of electrons of the thiourea amide nitrogen which lies between two partially positive carbon atoms (carbonyl and thiocarbonyl), since it might spend some of its time at the N–C=S bonds.

The two protons attached to the thiourea primary nitrogen are chemically not equivalent due to hindered amine rotation [40]. This is illustrated by the difference in their chemical shifts in the ^{1}H-NMR spectrum of **4** and **5** (0.3 ppm and 0.33 ppm respectively). Their peaks (9.34 and 9.64 ppm for **4** and 9.32 and 9.65 ppm for **5**), together with that of thiourea NH (11.06 ppm for **4** and 11.04 ppm for **5**), usually appear weak or do not appear at all when the concentration is low or during ^{1}H-NMR spectroscopy using d_6-DMSO as the solvent, since these protons could be considered as exchangeable protons with the residual D$_2$O [41,42].

3.2. Cytotoxicity Study

Compounds **4** and **5** were tested in vitro for antiproliferative activity against HRT-18 cell line (human colon adenocarcinoma), HC-04 cell line (mouse hepatic carcinoma), and HBL-100 cell line (epithelial cells obtained from healthy human breast milk) at micromolar concentrations (6.25, 12.5, 25, 50, 100 μM). Both of them showed inhibitory activity against the cancer cell lines higher than against the normal cell line. Figures 5 and 6 show that there is a continuous and parallel increase in the inhibition of growth exhibited by both compounds against both colon adenocarcinoma and hepatic carcinoma with increasing the concentration. On the other hand, they show low cytotoxicity against normal cells.
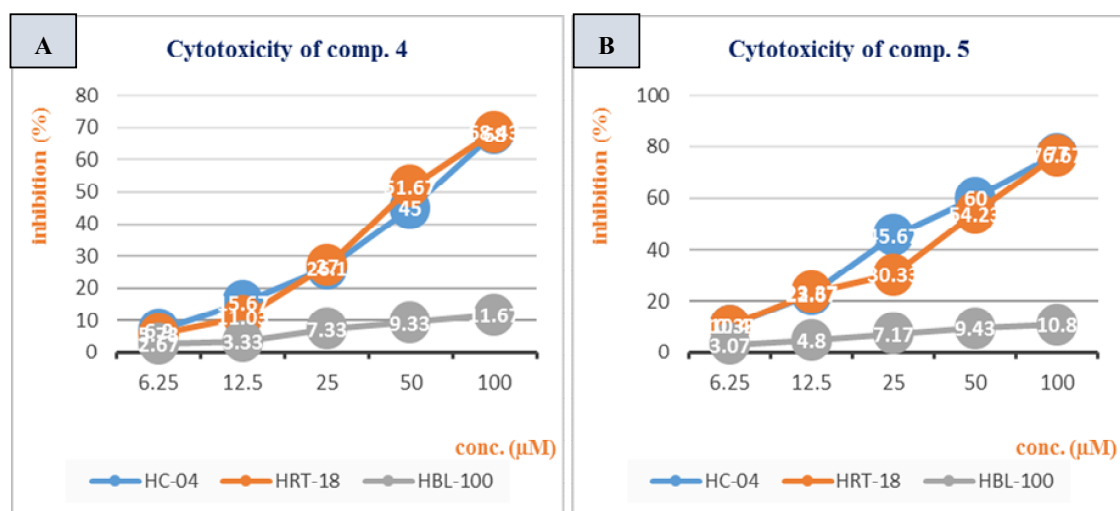

Figure 5. Concentration-growth inhibition curve of the tested compounds against hepatic carcinoma cells (blue), colon adenocarcinoma (orange), and healthy breast cells (gray). (**A**) The cytotoxicity of compound **4**; (**B**) The cytotoxicity of compound **5**.
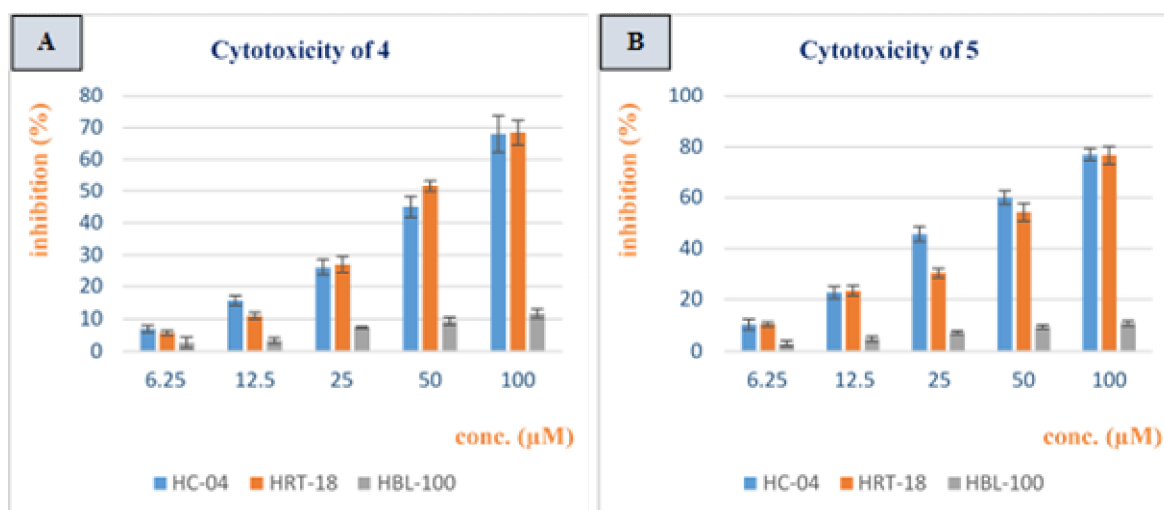
Figure 6. Histogram showing the concentration and growth inhibition of the tested compounds against hepatic carcinoma cells (blue), colon adenocarcinoma (orange), and healthy breast cells (gray). (**A**) The cytotoxicity of compound **4**; (**B**) The cytotoxicity of compound **5** (values are represented by the mean ± SEM of triplicate measurements).

Compound **5** was somewhat more cytotoxic than compound **4** against the tested cancer cells. Its IC_{50} against HC-04 cell line and HRT-18 cell line were 21.44 µM and 24.12 µM respectively while those for compound **4** were 27.37 µM and 30.42 µM. Figure 7 (captured at the IC_{50}) shows the difference in the magnitude of cytotoxicity between the two compounds.
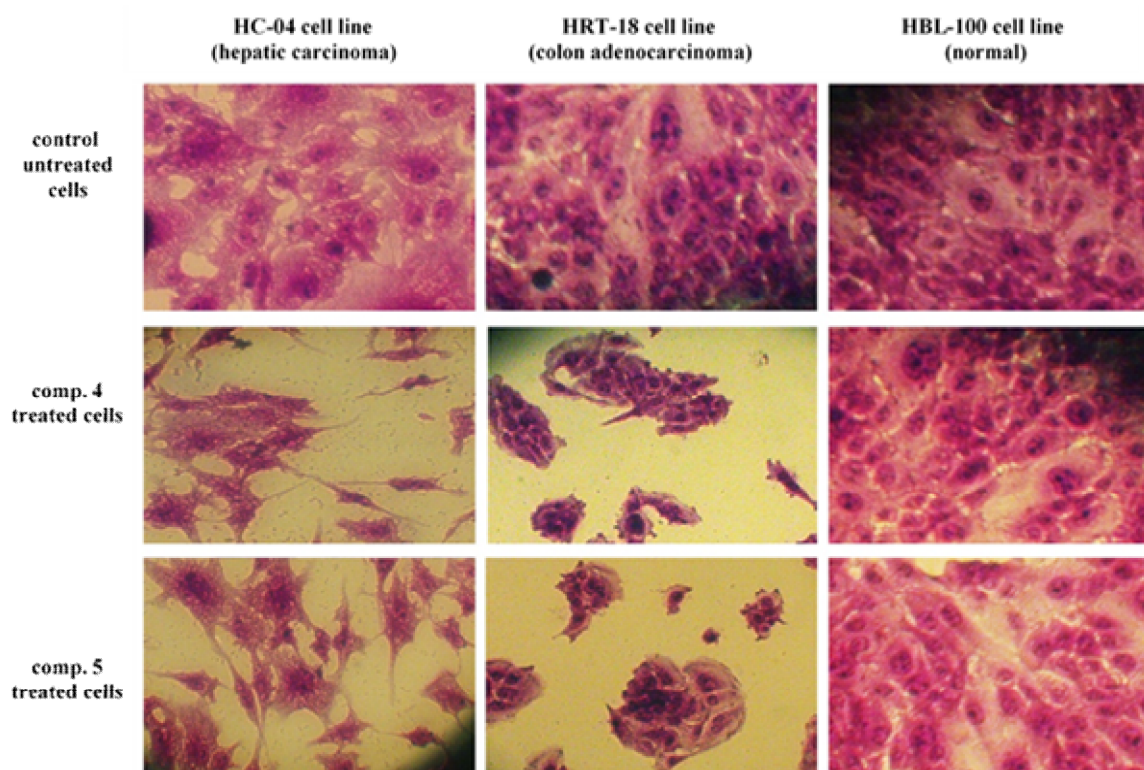

Figure 7. Morphology of the cell lines after treatment with compounds **4** and **5** at the IC_{50}. Scale bar is 50 µm.

Figure 8 illustrates a comparison between the cytotoxicity of these compounds against the tested cancer cell lines.
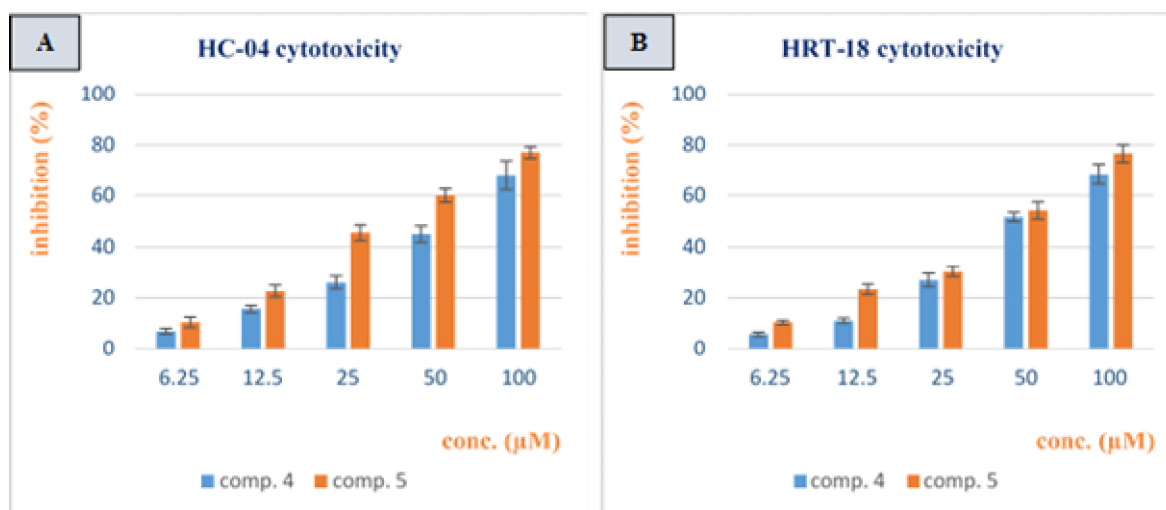

Figure 8. Histogram showing the concentration and growth inhibition of the compounds **4** and **5**, (**A**) against hepatic carcinoma cells and (**B**) against colon adenocarcinoma (values are represented by the mean ± SEM of triplicate measurements).

The low cytotoxicity of both compounds against normal cells gives hope of being able to target cancer cells to a higher degree than normal cells. No more than 12% of inhibition of growth was observed at the highest concentration used for both compounds (Figure 9). This might possibly be considered, in agreement with previous reports [3,4], that the synthesized compounds might exhibit relative specificity in inhibiting HDACs that are overexpressed in cancer cells. Besides, HDAC1 and HDAC2 are absent in normal breast cells [43,44] which further supports this low cytotoxicity in normal tissue. Furthermore, it was hypothesized that normal cells, in contrast to cancer cells, could withstand the inhibitory action of HDAC inhibitors and compensate for the inhibited vital pathways, since they have multiple, alternative epigenetic regulatory pathways [45].
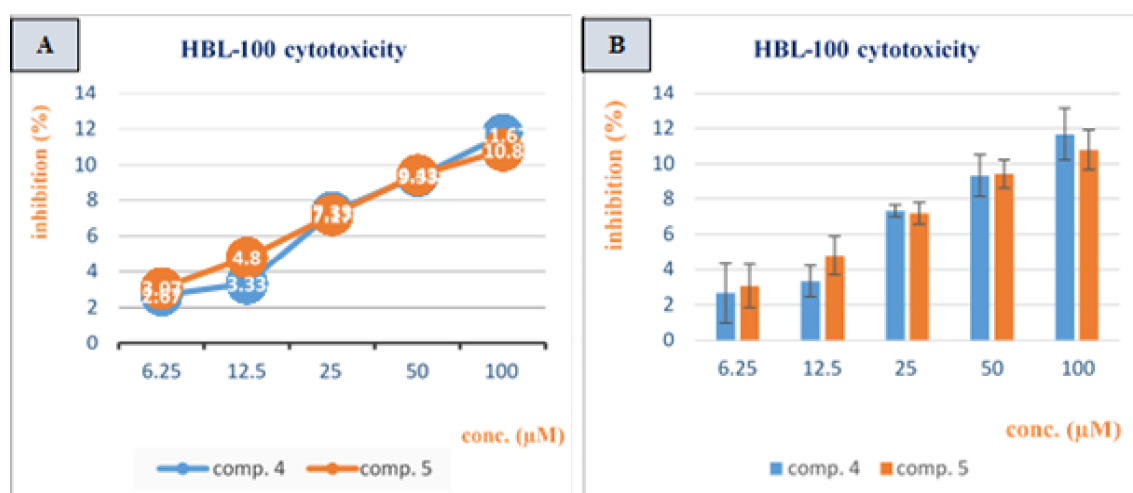

Figure 9. Low cytotoxicity of compounds **4** and **5** on normal breast cells. (**A**) Concentration-growth inhibition curve; (**B**) Histogram showing the concentration and growth inhibition (values are represented by the mean ± SEM of triplicate measurements).

These findings, besides our docking results (Section 3.3), support that our designed and synthesized compounds (**4** and **5**) are successful candidates to be HDAC inhibitors.

3.3. Docking Study

In order to get a preliminary confirmation that compounds **4** and **5** could be successful HDAC inhibitors, their inhibitory mode was simulated by a docking study against several isoforms of HDACs, the crystalline structures of which are confirmed and well resolved and the data of their binding modes to the co-crystallized ligands are available at the protein data bank (PDB, www.rcsb.org).

Compounds **4** and **5** together with SAHA (**1**), for comparison purposes, were docked against various isoforms of HDACs. These isoforms together with their pdb codes are HDAC1 (5ICN) [46], HDAC2 (4LXZ) [8], HDAC3 (4A69) [47], HDAC4 (5A2S) [48], HDAC7 (3ZNR) [49], HDAC8 (4QA0) [50], and HDAC10 (5TD7) [51].

For each docking, the parameters studied and compared were the binding free energy, the inhibition constant (K_i), number and length of hydrogen bonds between the ligand atoms and amino acid residues located in the binding site of the enzymes, and distance between ligand heteroatoms, which might contribute to zinc binding, and zinc ion of the enzyme.

Since compounds **4** and **5** have been designed to be inhibitors with ZBG, zinc ion was not removed during the enzyme preparation step before performing docking. Moreover, the preparation step included the addition of hydrogen atoms to the enzyme structure to simulate the biological pH (7.4) by correcting the oxidation and tautomeric states of the amino acid residues.

Docking experiments showed that compounds **4** and **5** have binding affinities comparable to, or better than, that of **1** with HDAC2 and HDAC7. The results of docking with these isoforms are summarized in Table 1. Images representing the ligand poses as well as hydrogen bond interactions between the ligand and the enzyme are listed in Supplementary File 2. To distinguish the atoms involved in hydrogen bonding, as well as heteroatoms, in the docked compounds, assignment numbers are given to these atoms (Figure 10).

Table 1. Docking results of compounds **4** and **5** against HDAC2 and HDAC7.

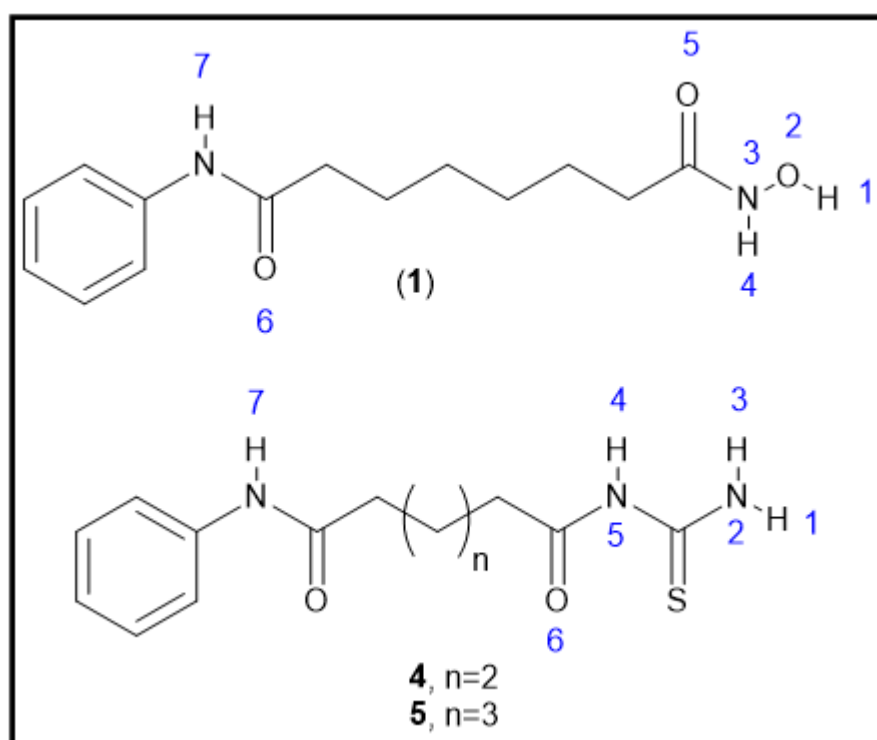| Isoform/PDB Code	Ligand	Pose Rank	Energy of Binding (Kcal/mol)	K_i	H-Bonds				Distance from Zn^{+2} (Å)
					no.	Involved Ligand Atoms	Involved Residue	Length (Å)	
HDAC2/4LXZ, chain A	SAHA	1st	−7.1	6.2×10^{-6}	1	1H	Tyr297	2.029	2O:5.117 5O:2.198
	4	1st	−7.3	4.42×10^{-6}	4	1H 3H 3H 4H	His135 Asp170(OD1) Asp170(OD2) Asp258	2.3 2.326 2.165 2.705	2N:2.028 S:3.890 6O:4.278
	5	1st	−7.1	6.2×10^{-6}	1	1H	Asp170	2.483	2N:2.012 S:3.889 6O:4.247
HDAC7/3ZNR, chain A	SAHA	6th	−6.9	8.69×10^{-6}	2	5O 5O	His137 His136	2.311 2.180	2O:5.314 5O:2.224
	4	3rd	−7.2	5.37×10^{-6}	4	1H 1H 1H 6O	Asp174(OD2) Asp174(OD1) Asp268 His176	2.343 2.204 2.308 2.152	2N:1.445 S:3.781 6O:4.819
	5	2nd	−7.2	5.37×10^{-6}	3	6O 1H S	Gly309 His176 His136	1.986 2.353 3.176	2N:2.555 S:3.693 6O:4.267

Figure 10. Assigned numbers to important atoms of the docked compounds.

The binding energies of compounds **4** and **5** are close to that of **1** when docked to HDAC2, −7.3, −7.1, and −7.1 kcal/mol respectively. Compound **4** has the highest number of hydrogen bonds, four. The 5O atom in **1** lies closer to the zinc ion than the 2O atom. The distance is 2.198 Å between the 5O atom and zinc ion whereas it is 5.117 Å between the 2O atom and zinc ion. The 2N and the S atoms of compounds **4** and **5** show closer distances to the zinc ion than those of **1** atom; 2.028 Å and 2.012 Å for the 2N atoms of compounds **4** and **5** respectively, and 3.890 Å and 3.889 Å for the S atom of compounds **4** and **5** respectively. This indicates that there is a high possibility for compounds **4** and **5** to coordinate zinc ion [52,53].

Results of docking **1** into HDAC7 showed that it was away from zinc ion in the first five poses. Similarly, **4** was away in the first two poses while **5** was away from zinc ion in the first pose. Accordingly, the binding energy of the sixth pose of **1** with HDAC7 is -6.9 kcal/mol whereas it is −7.2 kcal/mol for both **4** and **5** (third and second pose respectively). At these selected poses, compounds **1**, **4** and **5** exhibited two, four and three hydrogen bonds respectively with amino acid residues located near the end of the binding cavity. The carbonyl oxygen atom (5O) of **1** is 2.224 Å away from zinc ion while the distance between the 2N atom and zinc ion in **4** and **5** is 1.445 Å and 2.555 Å respectively. Furthermore, the S atom of compounds **4** and **5** is closer to the zinc ion than the oxygen atom of the hydroxyl group of **1** (2O); the distances are 3.693 Å and 3.781 Å for compounds **4** and **5** respectively while it is 5.314 Å for **1**.

Results of docking of **4** and **5** into HDAC2 are in agreement with their cytotoxicity results against the chosen cell lines. There is no large difference between the IC_{50} values of both **4** and **5** of the two cancer cell lines (HC-04 and HRT-18), not more than 3 μM (Figure 8). This is reflected by the equal binding energies of the two compounds when docked into HDAC2. Likewise, their low cytotoxicity against normal cell lines (Figure 9, HBL-100; epithelial cells obtained from healthy human breast milk) is reflected by the exhibited high affinity when docked into HDAC2 which is, as mentioned above, absent in normal breast cells. All these results collectively indicate that compounds **4** and **5** could be selective HDAC2 inhibitors with their acyl thiourea functionality acting as a novel, unique ZBG.

4. Conclusions

Synthesis of the target acyl thiourea derivatives (**4** and **5**) was achieved successfully starting from adipic acid (**4a**) and pimelic acid (**5a**) respectively. They exhibited cytotoxicity against cancer cell lines (HC-04 and HRT-18) that was higher than that exhibited against normal cell line (HBL-100). Their docking study, combined with cytotoxicity results, gave a preliminary indication that they are successful candidates to be HDAC inhibitors, having acyl thiourea functionality as a ZBG. Therefore, we are encouraged to extend our future research to include studying their pharmacokinetic profile, performing in vivo toxicity studies, and extending the cytotoxicity assay to include several cancer cell lines.

Supplementary Materials: The following are available online at http://www.mdpi.com/2218-0532/87/4/28/s1. Characterization spectra of the final compounds and intermediates (FT-IR, ^{1}H-NMR and ^{13}C-NMR) are provided in Supplementary File 1. Figures illustrating poses of the docked ligands into HDAC2 and HDAC7 and their hydrogen bonding are given in Supplementary File 2.

Author Contributions: Conceptualization and supervision, M.H.M.; investigation, methodology, and manuscript writing, D.H.A.-A.

Funding: This research received no external funding.

Conflicts of Interest: The authors declare no conflict of interest.

References

1. Seto, E.; Yoshida, M. Erasers of Histone Acetylation: The Histone Deacetylase Enzymes. Cold Spring Harbor Perspectives in Biology. *Cold Spring Harb Perspect Med.* **2014**, *6*, 18713.
2. Burtis, C.A.; Ashwood, E.R.; Bruns, D.E. *Tietz Textbook of Clinical Chemistry and Molecular Diagnostics*, Fifth ed.; Elsevier: Maryland Heights, MO, USA, 2012; pp. 1212–1214.
3. Delcuve, G.P.; Khan, D.H.; Davie, J.R. Targeting Class I Histone Deacetylases in Cancer Therapy. *Expert Opin. Ther. Targets* **2013**, *17*, 29–41. [CrossRef] [PubMed]
4. Cao, F.; Zwinderman, M.R.H.; Dekker, F.J. The Process and Strategy for Developing Selective Histone Deacetylase 3 Inhibitors. *Molecules* **2018**, *23*, 551. [CrossRef]
5. Zhang, L.; Zhang, J.; Jiang, Q.; Zhang, L.; Song, W. Zinc Binding Groups for Histone Deacetylase Inhibitors. *J. Enzym. Inhib. Med. Chem.* **2018**, *33*, 714–721. [CrossRef]
6. Li, Z.; Zhu, W.G. Targeting Histone Deacetylases for Cancer Therapy: From Molecular Mechanisms to Clinical Implications. *Int. J. Biol. Sci.* **2014**, *10*, 757–770. [CrossRef]
7. Kim, H.-J.; Bae, S.-C. Histone Deacetylase Inhibitors: Molecular Mechanisms of Action and Clinical Trials as Anti-Cancer Drugs. *Am. J. Transl. Res.* **2011**, *3*, 166–179.
8. Lauffer, B.E.L.; Mintzer, R.; Fong, R.; Mukund, S.; Tam, C.; Zilberleyb, I.; Flicke, B.; Ritscher, A.; Fedorowicz, G.; Vallero, R.; et al. Histone Deacetylase (HDAC) Inhibitor Kinetic Rate Constants Correlate with Cellular Histone Acetylation but Not Transcription and Cell Viability. *J. Biol. Chem.* **2013**, *288*, 26926–26943. [CrossRef]
9. Wang, D.F.; Helquist, P.; Wiech, N.L.; Wiest, O. Toward Selective Histone Deacetylase Inhibitor Design: Homology Modeling, Docking Studies, and Molecular Dynamics Simulations of Human Class I Histone Deacetylases. *J. Med. Chem.* **2005**, *48*, 6936–6947. [CrossRef]
10. Bieliauskas, A.V.; Pflum, M.K.H. Isoform-Selective Histone Deacetylase Inhibitors. *Chem. Soc. Rev.* **2008**, *37*, 1402–1413. [CrossRef]
11. Manal, M.; Chandrasekar, M.J.N.; Gomathi Priya, J.; Nanjan, M.J. Inhibitors of Histone Deacetylase as Antitumor Agents: A Critical Review. *Bioorg. Chem.* **2016**, *67*, 18–42. [CrossRef]
12. Marks, P.A. Discovery and Development of SAHA as an Anticancer Agent. *Oncogene* **2007**, *26*, 1351–1356. [CrossRef] [PubMed]
13. Mann, B.S.; Johnson, J.R.; Cohen, M.H.; Justice, R.; Pazdur, R. FDA Approval Summary: Vorinostat for Treatment of Advanced Primary Cutaneous T-Cell Lymphoma. *Oncologist* **2007**, *12*, 1247–1252. [CrossRef] [PubMed]

14. Binzet, G.; Külcü, N.; Flörke, U.; Arslan, H. Synthesis and Characterization of Cu(II) and Ni(II) Complexes of Some 4-Bromo-*N*-(Di(Alkyl/Aryl)Carbamothioyl) Benzamide Derivatives. *J. Coord. Chem.* **2009**, *62*, 3454–3462. [CrossRef]

15. Saeed, S.; Rashid, N.; Jones, P.; Hussain, R. Thermomechanical Studies of Thermally Stable Metal-Containing Epoxy Polymers from Diglycidyl Ether of Bisphenol A and Amino-Thiourea Metal Complexes. *Eur. J. Chem.* **2011**, *2*, 77–82. [CrossRef]

16. Selvakumaran, N.; Sandhiya, L.; Bhuvanesh, N.S.P.; Senthilkumar, K.; Karvembu, R. Structural Diversity in Aroylthiourea Copper Complexes-Formation and Biological Evaluation of [Cu(i)(μ-S)SCl]$_2$,: Cis -Cu(II)S$_2$O$_2$, Trans -Cu(II)S$_2$O$_2$ and Cu(i)S$_3$ Cores. *New J. Chem.* **2016**, *40*, 5401–5413. [CrossRef]

17. Gandhaveeti, R.; Konakanchi, R.; Jyothi, P.; Bhuvanesh, N.S.P.; Anandaram, S. Unusual Coordination Mode of Aroyl/Acyl Thiourea Ligands and Their π-Arene Ruthenium (II) Piano-Stool Complexes: Synthesis, Molecular Geometry, Theoretical Studies and Biological Applications. *Appl. Organometal. Chem.* **2019**, *33*, 1–13. [CrossRef]

18. Parmar, S.; Kumar, Y.; Mittal, A. Synthesis, Spectroscopic and Pharmacological Studies of Bivalent Copper, Zinc and Mercury Complexes of Thiourea. *S. Afr. J. Chem.* **2010**, *63*, 123–129.

19. Prakash, J.T.J.; Nirmala, L.R. Synthesis, Spectral and Thermal Properties of Bis Thiourea Zinc Acetate (BTZA) Nonlinear Optical Single Crystal. *Int. J. Comput. Appl.* **2010**, *8*, 7–11. [CrossRef]

20. Swaminathan, K.; Irving, H.M.N.H. Infra-Red Absorption Spectra Complexes of Thiourea. *J. Inorg. Nucl. Chem.* **1964**, *26*, 1291–1294. [CrossRef]

21. Trott, O.; Olson, A.J. AutoDock Vina: Improving the Speed and Accuracy of Docking with a New Scoring Function, Efficient Optimization, and Multithreading. *J. Comput. Chem.* **2010**, *31*, 455–461. [CrossRef]

22. Pettersen, E.F.; Goddard, T.D.; Huang, C.C.; Couch, G.S.; Greenblatt, D.M.; Meng, E.C.; Ferrin, T.E. UCSF Chimera–a Visualization System for Exploratory Research and Analysis. *J. Comput. Chem.* **2004**, *25*, 1605–1612. [CrossRef] [PubMed]

23. Berman, H.M.; Westbrook, J.; Feng, Z.; Gilliland, G.; Bhat, T.N.; Weissig, H.; Shindyalov, I.N.; Bourne, P.E. The Protein Data Bank. *Nucleic Acids Res.* **2000**, *28*, 235–242. [CrossRef] [PubMed]

24. Sulaiman, G.M.; Jabir, M.S.; Hameed, A.H. Nanoscale Modification of Chrysin for Improved of Therapeutic Efficiency and Cytotoxicity. *Artif. Cells Nanomed. Biotechnol.* **2018**, *46* (Suppl. 1), 708–720. [CrossRef] [PubMed]

25. Jabir, M.S.; Taha, A.A.; Sahib, U.I.; Taqi, Z.J.; Al-Shammari, A.M.; Salman, A.S. Novel of Nano Delivery System for Linalool Loaded on Gold Nanoparticles Conjugated with CALNN Peptide for Application in Drug Uptake and Induction of Cell Death on Breast Cancer Cell Line. *Mater. Sci. Eng. C* **2019**, *94*, 949–964. [CrossRef] [PubMed]

26. Sinko, P. *Martin's Physical Pharmacy and Pharmaceutical Sciences. Physical Chemical and Biopharmaceutical Principles in the Pharmaceutical Sciences*; Lippincott Williams & Wilkins: Baltimore, MD, USA, 2011; p. 74.

27. Herman, D.; Jenssen, K.; Burnett, R.; Soragni, E.; Perlman, S.L.; Gottesfeld, J.M. Histone Deacetylase Inhibitors Reverse Gene Silencing in Friedreich's Ataxia. *Nat. Chem. Biol.* **2006**, *2*, 551–558. [CrossRef]

28. Hill, J.W. Studies on polymerization and ring formation. Vi. Adipic anhydride. *J. Am. Chem. Soc.* **1930**, *52*, 4110–4114. [CrossRef]

29. Stowell, J.C.; Huot, R.I.; Van Voast, L. The Synthesis of *N*-Hydroxy-*N'*-Phenyloctanediamide and Its Inhibitory Effect on Proliferation of AXC Rat Prostate Cancer Cells. *J. Med. Chem.* **1995**, *38*, 1411–1413. [CrossRef]

30. Letton, J.C.; Miller, L.E. Process for the Preparation of Mono-Condensation Derivatives of Adipic Acid. U.S. Patent 5286879A, 15 February 1994.

31. Wolfe, S.; Godfrey, J.C.; Holdrege, C.T.; Perron, Y.G. Rearrangement of Penicillins to Anhydropenicillins. *Can. J. Chem.* **1968**, *46*, 2549–2559. [CrossRef]

32. Khairul, W.M.; Daud, A.I.; Mohd Hanifaah, N.A.; Arshad, S.; Razak, I.A.; Zuki, H.M.; Erben, M.F. Structural Study of a Novel Acetylide-Thiourea Derivative and Its Evaluation as a Detector of Benzene. *J. Mol. Struct.* **2017**, *1139*, 353–361. [CrossRef]

33. Klayman, D.L.; Shine, R.J.; Bower, J.D. The Reaction of S-Methiodide Derivatives of Activated Thioureas with Hydroxylic Compounds. A Novel Synthesis of Mercaptans. *J. Org. Chem.* **1972**, *37*, 1532–1537. [CrossRef]

34. Furniss, B.S.; Hannaford, A.J.; Smith, P.W.G.; Tatchell, A.R. *Vogel's Textbook of Practical Organic Chemistry*, Fifth ed.; Longman Scientific & Technical: Harlow, UK, 1989; pp. 416–417.

35. Smith, J.F.; Li, C.; Roth, M.; Hepler, L.G. Solubility of Ammonia in Chloroform: Analysis in Terms of Henry's Law and the Equilibrium Constant for Hydrogen-Bonded Complex Formation. *Can. J. Chem.* **1989**, *67*, 2213–2217. [CrossRef]

36. Dixon, E. The Constitution of "Thiocyanates" Containing an Electronegativc Group. *J. Chem. Soc. Trans.* **1908**, *93*, 684–700. [CrossRef]

37. Wu, J.; Shi, Q.; Chen, Z.; He, M.; Jin, L.; Hu, D. Synthesis and Bioactivity of Pyrazole Acyl Thiourea Derivatives. *Molecules* **2012**, *17*, 5139–5150. [CrossRef] [PubMed]

38. Zhong, Z.; Xing, R.; Liu, S.; Wang, L.; Cai, S.; Li, P. Synthesis of Acyl Thiourea Derivatives of Chitosan and Their Antimicrobial Activities in Vitro. *Carbohydr. Res.* **2008**, *343*, 566–570. [CrossRef]

39. Bai, L.; Li, K.; Li, S.; Wang, J.-X. Phase Transfer Catalytic Synthesis of Phenylacetyl Arylthioureas Under Microwave Irradiation Conditions. *Synth. Commun.* **2002**, *32*, 1001–1007. [CrossRef]

40. Gorobets, N.Y.; Yermolayev, S.A.; Gurley, T.; Gurinov, A.A.; Tolstoy, P.M.; Shenderovich, I.G.; Leadbeater, N.E. Difference between ^{1}H NMR Signals of Primary Amide Protons as a Simple Spectral Index of the Amide Intramolecular Hydrogen Bond Strength. *J. Phys. Org. Chem.* **2012**, *25*, 287–295. [CrossRef]

41. Chayah, M.; Camacho, M.E.; Carrión, M.D.; Gallo, M.A. ^{1}H and ^{13}C NMR Spectral Assignment of N,N'-Disubstituted Thiourea and Urea Derivatives Active against Nitric Oxide Synthase. *Magn. Reson. Chem.* **2016**, *54*, 793–799. [CrossRef]

42. Firdausiah, S.; Hasbullah, S.A.; Yamin, B.M. Synthesis, Structurale Elucidation and Antioxidant Study of Ortho- Substituted N, N ' -Bis (Benzamidothiocarbonyl) Hydrazine Derivatives. *J. Phys. Conf. Ser.* **2018**, *979*, 012010. [CrossRef]

43. De Ruijter, A.J.M.; van Gennip, A.H.; Caron, H.N.; Kemp, S.; van Kuilenburg, A.B.P. Histone Deacetylases (HDACs): Characterization of the Classical HDAC Family. *Biochem. J.* **2003**, *370*, 737–749. [CrossRef]

44. Zhou, H.; Wang, C.; Ye, J.; Chen, H.; Tao, R. Design, Virtual Screening, Molecular Docking and Molecular Dynamics Studies of Novel Urushiol Derivatives as Potential HDAC2 Selective Inhibitors. *Gene* **2017**, *637*, 63–71. [CrossRef]

45. Eckschlager, T.; Plch, J.; Stiborova, M.; Hrabeta, J. Histone Deacetylase Inhibitors as Anticancer Drugs. *Int. J. Mol. Sci.* **2017**, *18*, 1414. [CrossRef] [PubMed]

46. Watson, P.J.; Millard, C.J.; Riley, A.M.; Robertson, N.S.; Wright, L.C.; Godage, H.Y.; Cowley, S.M.; Jamieson, A.G.; Potter, B.V.L.; Schwabe, J.W.R. Insights into the Activation Mechanism of Class I HDAC Complexes by Inositol Phosphates. *Nat. Commun.* **2016**, *7*, 11262. [CrossRef] [PubMed]

47. Watson, P.J.; Fairall, L.; Santos, G.M.; Schwabe, J.W.R. Structure of HDAC3 Bound to Co-Repressor and Inositol Tetraphosphate. *Nature* **2012**, *481*, 335–340. [CrossRef] [PubMed]

48. Luckhurst, C.A.; Breccia, P.; Stott, A.J.; Aziz, O.; Birch, H.L.; Bürli, R.W.; Hughes, S.J.; Jarvis, R.E.; Lamers, M.; Leonard, P.M.; et al. Potent, Selective, and CNS-Penetrant Tetrasubstituted Cyclopropane Class IIa Histone Deacetylase (HDAC) Inhibitors. *ACS Med. Chem. Lett.* **2016**, *7*, 34–39. [CrossRef]

49. Lobera, M.; Madauss, K.P.; Pohlhaus, D.T.; Wright, Q.G.; Trocha, M.; Schmidt, D.R.; Baloglu, E.; Trump, R.P.; Head, M.S.; Hofmann, G.A.; et al. Selective Class IIa Histone Deacetylase Inhibition via a Nonchelating Zinc-Binding Group. *Nat. Chem. Biol.* **2013**, *9*, 319–325. [CrossRef]

50. Decroos, C.; Bowman, C.M.; Moser, J.A.S.; Christianson, K.E.; Deardorff, M.A.; Christianson, D.W. Compromised Structure and Function of HDAC8 Mutants Identified in Cornelia de Lange Syndrome Spectrum Disorders. *ACS Chem. Biol.* **2014**, *9*, 2157–2164. [CrossRef]

51. Hai, Y.; Shinsky, S.A.; Porter, N.J.; Christianson, D.W. Histone Deacetylase 10 Structure and Molecular Function as a Polyamine Deacetylase. *Nat. Commun.* **2017**, *8*, 15368. [CrossRef]

52. Jones, P.; Bottomley, M.J.; Carfí, A.; Cecchetti, O.; Ferrigno, F.; Lo Surdo, P.; Ontoria, J.M.; Rowley, M.; Scarpelli, R.; Schultz-Fademrecht, C.; et al. 2-Trifluoroacetylthiophenes, a Novel Series of Potent and Selective Class II Histone Deacetylase Inhibitors. *Bioorg. Med. Chem. Lett.* **2008**, *18*, 3456–3461. [CrossRef]

53. Abdel-Atty, M.M.; Farag, N.A.; Kassab, S.E.; Serya, R.A.T.; Abouzid, K.A.M. Design, Synthesis, 3D Pharmacophore, QSAR, and Docking Studies of Carboxylic Acid Derivatives as Histone Deacetylase Inhibitors and Cytotoxic Agents. *Bioorg. Chem.* **2014**, *57*, 65–82. [CrossRef]